Jitonnom, J., Mujika, J. I., van der Kamp, M. W., & Mulholland, A. J. (2017). Quantum mechanics/molecular mechanics simulations identify the ring-opening mechanism of creatininase. *Biochemistry*, *56*(48), 6377-6388. https://doi.org/10.1021/acs.biochem.7b01032

QM/MM Simulations Identify the Ring-Opening Mechanism of Creatininase

Jitrayut Jitonnom*[†], Jon I. Mujika[‡], Marc W. van der Kamp[ǁ,§], and Adrian J. Mulholland[§]

[†] Division of Chemistry, School of Science, University of Phayao, Phayao, 56000 Thailand

[‡] Kimika Fakultatea, Euskal Herriko Unibertsitatea UPV/EHU, and Donostia International Physics Center (DIPC), P.K. 1072, 20080 Donostia, Euskadi, Spain

[ǁ] School of Biochemistry, Biomedical Sciences Building, University Walk, University of Bristol, BS8 1TD, U.K.

[§] Centre for Computational Chemistry, School of Chemistry, University of Bristol, Bristol BS8 1TS, U.K.

To whom correspondence should be addressed: J.J.: Tel: +66 (0) 5446 6666 ext. 1834; Fax: +66 (0) 5446 6664. E-mail: jitrayut.018@gmail.com

Abstract

Creatininase catalyzes the conversion of creatinine (a biosensor for kidney function) to creatine via a two-step mechanism: water-addition followed by ring-opening. Water-addition is common to other known cyclic amidohydrolases, but the precise mechanism for ring-opening is still under debate. The proton donor in this step is either His178, or a water molecule bound to one of metal ions, and the roles of His178 and Glu122 are unclear. Here, the two possible reaction pathways have been fully examined by means of combined quantum mechanics/molecular mechanics simulations at the SCC-DFTB/CHARMM22 level of theory. The results indicate that His178 is the main catalytic residue for the whole reaction and explain its role as proton shuttle during the ring-opening step. In the first step, His178 provides electrostatic stabilization to the *gem-diolate* tetrahedral intermediate. In the second step, His178 abstracts the hydroxyl proton of the intermediate and delivers it to the cyclic amide nitrogen, leading to ring-opening. The latter is the rate-limiting step with a free energy barrier of 18.5 kcal/mol, in agreement with the experiment. We find that Glu122 must be protonated during the enzyme reaction, so that it can form a stable hydrogen bond with its neighbouring water molecule. Simulations of the mutant E122Q showed that this replacement disrupts the H-bond network formed by three conserved residues (Glu34, Ser78, and Glu122) and water, increasing the energy barrier. Our computational studies provide a comprehensive explanation for previous structural and kinetic observations, including why H178A causes a complete loss of activity but E122Q does not.

Keywords: QM/MM; creatininase, enzyme catalysis; SCC-DFTB; zinc metalloenzyme; free energy

1. Introduction

Creatininase (creatinine amidohydrolase; EC 3.5.2.10), belonging to a member of the urease-related amidohydrolase superfamily [1, 2], catalyzes the reversible interconversion of creatinine to creatine (see Scheme 1), specifically acting on carbon-nitrogen bonds in cyclic amides, like dihydroorotase [3] and other cyclic amidohydrolases [4]. The enzyme plays a key role in the bacterial degradation of creatinine [5] and participates in arginine and proline metabolism [6]. With growing industrial demand, considerable efforts have been made for decades to characterize the properties of creatininase from various microorganisms, including the bacterial enzyme from *Pseudomonas putida* [2, 7-12]. Since the first X-ray crystal structure of creatininase was reported in late 2002 by Beuth *et al.* [9], several structures have been characterized to understand the structure and function of the enzyme [9-12]. The structures showed that creatininase has a unique structural fold $(\beta\alpha)_4$ compared to that of other members of urease-related amidohydrolase superfamily [2], containing a binuclear metal center in each subunit. Usually, two zinc ions are located at the M1 and M2 sites (hereafter called Zn1 and Zn2, respectively) within the active site, ligated by five conserved amino acid residues (Glu34, His36, Asp45, His120, Glu183) and two water molecules [10] (see Scheme 2). The two zinc ions are bridged by a bidentate interaction with Asp45, which is functionally equivalent to a carboxylated lysine residue found in related amidohydrolases, and by a zinc-bound water molecule that is activated as a hydroxide ion during catalysis.

Scheme 1: Creatininase-catalyzed ring-opening reaction

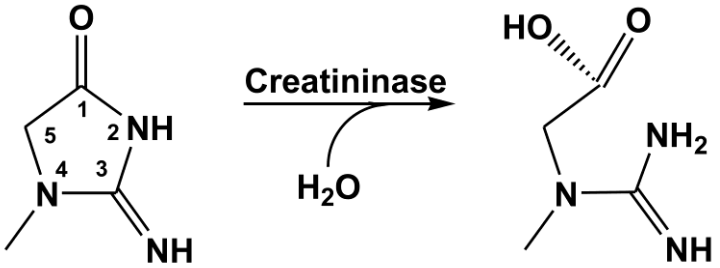

Scheme 2: Two previously proposed reaction mechanism for creatinine hydrolysis catalyzed by creatininase

Path I: Histidine-promoted ring-opening pathway (Beuth *et al.*) [10]

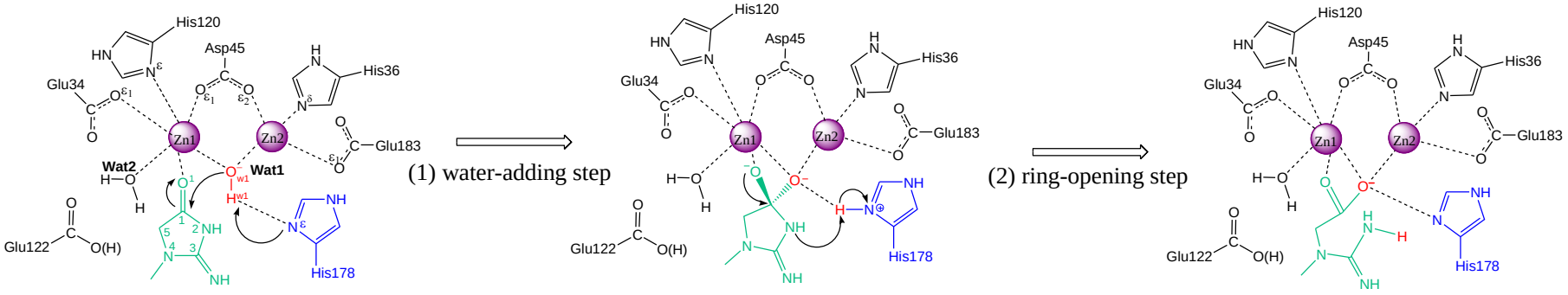

Path II: Water-promoted ring-opening pathway (Yoshimoto *et al.*) [12]

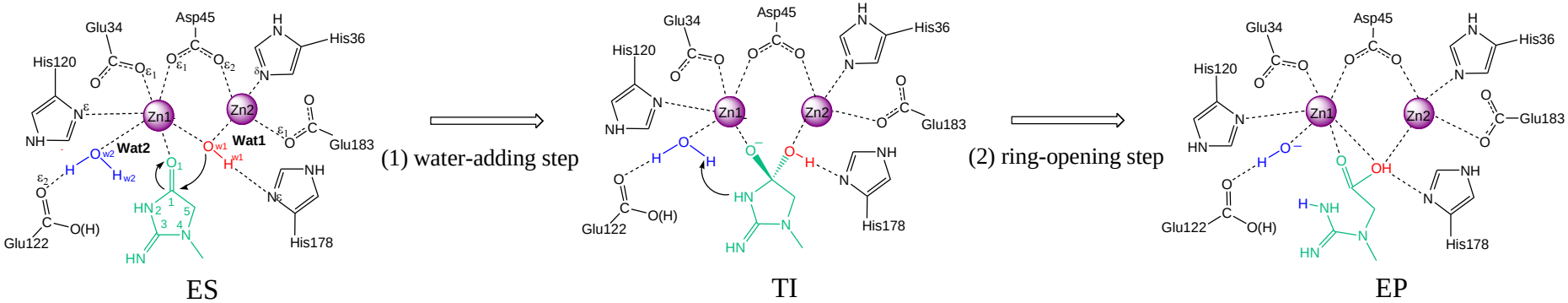

The crystal structures show different coordination geometries of M1 for each metal type, while M2, usually a zinc ion, shares a common tetrahedral coordination. In native creatininase (Zn-Zn enzyme), Zn1 has a distorted tetrahedral geometry bound to three protein ligands, namely, Glu34, Asp45, and His120, a carbonyl oxygen of creatinine substrate and a water molecule (Wat1). Zn2 has a well-ordered tetrahedral geometry bound to three protein ligands, namely, His36, Asp45, and Glu183 and Wat1. The first metal Zn1 can be replaced with other divalent cations (*e.g.*, Mn^{2+}, Mg^{2+}or Co^{2+}), providing highly active forms of the enzyme [13]. In a Mn-activated enzyme (Mn-Zn enzyme), Mn1 has a square-pyramidal geometry bound to the three protein ligands, the substrate and two water molecules (Wat1 and Wat2). Currently, a total of thirteen crystal structures of the enzyme are deposited in the Protein Data Bank (PDB), including the native enzyme [9, 10] and the enzyme-inhibitor/product complex [11, 12], but none of them have a substrate bound. The lack of structural information for the Michaelis complex could lead to an incomplete understanding of the catalytic mechanism of creatininase.

On the basis of the available X-ray structures [10-12], it is thought that the enzyme degrades creatinine via a two-step mechanism, similar to the urease-related amidohydrolase enzymes, such as urease [14], phosphotriesterase [15], dihydroorotase [3, 16] and of the aminopeptidases [17]. Specifically, these metalloenzymes initiate the addition of the nucleophilic water molecule that is located between the two metal ions (Wat1) followed by a ring-opening step assisted by a conserved aspartate/glutamate residue that functions as a catalytic base/acid [2]. In creatininase, the first step is likely to follow the same reaction mechanism, but in the second step two possible ring-opening pathways have been proposed for protonating the leaving amide group and concomitant carbon-nitrogen bond cleavage (see Scheme 2). They differ in the nature of the proton donor: either a protein residue (His178) [10] or a neighboring water molecule (Wat2) [11, 12] that is located between Glu122 and Zn1 could

play this role. His178 is located in a mobile flap (residues 168–180) that can be in an open or closed conformation, while Glu122 is located at the M1 site. His178 and Glu122, as well as other residues (Ser78, Tyr121, Trp154, Trp174) around the active site pocket (see Figure S1), also influence the creatininase activities [12].

Based on a theoretical model of the creatine-water adduct [10], His178 was proposed to act as catalytic base/acid (see Scheme 2), functionally similar to other analogous residues, *e.g.*, Asp315 in D-hydantoidase [18] or Glu131 in aminopeptidase [19], respectively. The catalytic role of His178 was confirmed by the total inhibition of the enzyme activity observed with the H178A mutant [12]. Alternatively, based on a high-resolution X-ray structure of product complex [11], it was suggested that a water molecule (Wat2), which forms a hydrogen bond with Glu122 and preferably binds M1, might play a crucial role as an acid catalyst (see Scheme 2). A possible catalytic role of Wat2 and Glu122 has also been demonstrated by the E122Q mutant [12], which showed a drastic decrease in the catalytic activity with one metal ion missing at M1. Nevertheless, the consequence of this structural change and the way by which the role of Glu122 in the reaction, and the causes of the effects of the E122Q mutation on the reaction, are still unknown. Previously, our group carried out a theoretical study to understand the influence of the metal cofactors and the water in the creatininase mechanism [20] but several key questions regarding the roles of active site residues and mechanistic issue still remain to be addressed: i) which residue (His178 or Wat2) would serve as the proton donor in the ring-opening step?, ii) Why does the E122Q mutant decrease the activity of creatininase but not abolish it?, iii) What is the specific role of Glu122 and its water solvent partner, Wat2, in the catalytic reaction?, iv) What is the protonation state of Glu122 and does this impact on the stability of the Glu122-Wat2 interaction? All of these questions emphasize the need of more studies in order to clarify the mechanism of the binuclear zinc enzyme creatininase and the roles of the catalytic residues.

In this paper, we examine the two mechanistic proposals (path I and II, Scheme 2) using a combined quantum mechanics/molecular mechanics (QM/MM) approach based on self-consistent charge density functional tight binding (SCC-DFTB) method. The complete free-energy profiles for the reaction pathways of wildtype (WT) and mutant (E122Q) creatininase were obtained using adiabatic mapping approach, in conjunction with the umbrella sampling technique. We have demonstrated the importance of the second-shell residues His178 and Glu122, as well as the roles of two active site water molecules observed in the X-ray structure and in catalysis. Furthermore, the molecular origin for the activity of the E122Q mutant was also described, in supporting the previous experimental finding.

2. Computational methods

2.1 Model preparation

Because of the absence of a X-ray crystal structure of the Michaelis complex, we constructed the wildtype creatininase model based on a high-resolution (1.6 Å) X-ray structure of the enzyme-product (EP) complex of Mn-activated creatininase (PDB entry 1V7Z [11]), a typical binuclear zinc metalloenzyme with one zinc ion substituted by a manganese ion, Mn^{2+}, (known as a Mn-Zn enzyme). The creatinine substrate was built from the creatine product in the X-ray structure by manually adjusting the C-N bond (see C_1–N_2, Scheme 1) to form a five-membered ring. One oxygen atom of creatine that is bridged with the two metals was replaced by a hydroxide ion, serving as the water nucleophile. The Mn atom was replaced by Zn to create a Zn-Zn wildtype enzyme model. All crystallographic water molecules were kept. Hydrogen atoms were added using the HBUILD subroutine in CHARMM and titratable residues in the enzyme were assigned based on the pK_a estimated by PROPKA 3.0 [21] at physiological pH. Because the interaction between the Glu122 residue and Wat2 remains unclear, we modeled Glu122 in both neutral and ionized forms. This will

help in clarifying the most likely protonation state of this important residue, as mentioned above. All other aspartate and glutamate residues were treated as deprotonated. His38, located outside the active site, was treated as doubly protonated, while other histidine residues were modeled in their neutral states, with their tautomeric state assigned on the basis of the hydrogen bonding network using WHAT-IF (http://swift.cmbi.ru.nl) [22]. The model for the E122Q mutant was obtained following the same steps as for the WT model, but replacing the –COOH in the Glu122 side-chain with $–CONH_2$, transforming it to glutamine.

2.2 QM/MM setup and QM/MM MD simulations

To set up the QM/MM calculations, the enzyme model must be partitioned into two regions: QM and MM. The QM region (see Scheme 2) consists of the substrate, the hydroxide ion (Wat1), and the two zinc ions along with the side chain groups of His36, His120, His178, Glu34, Glu/Gln122, Glu183 and the bridging Asp45 (truncated at the C_β atom of His and Asp and at the C_γ atom of Glu). In addition, a crystallographic water molecule (Wat2) near Glu122, which is thought to be important for catalysis [12], was also included in the QM region. The resulting QM regions of WT contain 86 (ionized Glu122) or 87 atoms (neutral Glu122) with a net charge of –1 and 0, respectively. The E122Q QM region comprises of 88 atoms and a net charge of 0. The QM region is described by an approximate density functional approach, namely the self-consistent charge density functional tight binding (SCC-DFTB) method [23] while the MM region accounting for the protein environment and water molecules is described by the CHARMM22 force field for proteins [24] and with the TIP3P water model [25]. The SCC-DFTB Hamiltonian has been parameterized for biological zinc ions [26], and the combined SCC-DFTB/CHARMM approach [27] has been shown to give a reasonably accurate description of several zinc enzymes [28-32].

Three QM/MM MD simulations were conducted: two WT systems (both neutral and ionized Glu122) and one of the E122Q mutant system using the same protocols applied successfully in our recent studies [33, 34]. In brief, the enzyme-substrate (ES) complex was solvated by a 25 Å radius sphere of pre-equilibrated TIP3P model waters centered on the carbonyl carbon atom (C_1) of substrate (see Scheme 1). A spherical deformable boundary potential [35] with a 25 Å radius was used to prevent the water from diffusing away from the system. All atoms outside the 25 Å sphere centered on the C_1 carbon were deleted, while protein heavy atoms in the buffer zone (21–25 Å) were subject to Langevin dynamics with positional restraints using force constants scaled to increase from the inside to the outside of the buffer. All atoms within a 21 Å sphere of the reaction zone were subjected to Newtonian dynamics with no positional restraints. The ES complex for each system was thermalized in the NVT ensemble at 310 K with 1200 ps of stochastic boundary QM/MM MD simulation, following the procedure described in refs [33, 34]. An integration time-step of 1 fs was used, with all of the bonds involving hydrogen atoms constrained using the SHAKE algorithm [36]. The EP complexes, which were taken from the final stage of the ring-opening step of the two pathways (path I and II, Scheme 2) during the adiabatic mapping calculations below, were also simulated using the same protocol as in the case of the ES. All simulations were performed using the CHARMM suite of programs [37].

2.3 QM/MM free energy calculations

From the QM/MM MD simulations of WT and E122Q, we picked up representative structures as starting points for modeling creatininase reactivities. Several snapshots were taken from the equilibrated QM/MM MD simulations (700 – 1200 ps) to ensure a diverse range of ES conformations, which was found to be important for other enzyme studies [33, 38, 39]. These initial geometries were subsequently minimized with the QM/MM Hamiltonian and

the Adopted Basis Newton-Raphson method (until the gradient < 0.01 kcal $mol^{-1}Å^{-1}$) to be afterwards used as starting points for SCC-DFTB/CHARMM22 adiabatic mapping calculations [40]. The reaction coordinates (RC) for the first water-adding and second ring-opening steps of path I and II in Scheme 2 were defined as linear combinations of interatomic distances as follows. For the first step, identical for both pathways, the RC is given by the distance between the water oxygen (O_{w1}) and the substrate carbonyl carbon (C_1): $RC_1 = d_{Ow1\cdots C1}$. In the second step, different sets of RCs were defined differently for path I and II (note that two steps are considered for path I): $RC_{2\text{-}I}$ (path I) = $d_{Ow1\cdots Hw1} - d_{Hw1\cdots N\varepsilon}$ (from −1.1 Å to 0.8 Å to facilitate the transfer of the *gem-diolate* proton to His178) and $RC_{3\text{-}I}$ (path I) = $d_{Hw1\cdots N\varepsilon} - d_{Hw1\cdots N2}$ (from −1.1 Å to 1.1 Å to facilitate the transfer of the proton from His178 to leaving nitrogen) while $RC_{2\text{-}II}$ (path II) = $d_{Ow2\cdots Hw2} - d_{Hw2\cdots N2} - d_{Ow2\cdots H\varepsilon}$ (from −3.8 Å to −0.8 Å to facilitate the transfer of the proton from Wat2 to leaving nitrogen). Details of all reaction coordinates are also illustrated in Figure S2 of the Supporting Information. Potential energy surfaces were characterized and the geometries representing the minimum energy pathway through the surfaces were used as the putative RC for the free-energy (potential of mean force) calculations, which allow a better conformational sampling along the reaction pathways and accounting for thermal fluctuations of the protein and solvent environment.

The free energies for each reaction pathway were computed based on the putative RCs with the QM/MM umbrella sampling MD simulations requiring a series of simulations to be performed with the harmonically restrained RC (utilizing a force constant of 200 kcal mol^{-1} $Å^{-2}$). All other variables of the umbrella sampling simulations were unchanged with respect to those used for the QM/MM MD simulations described above. Each simulation (window) consisted of 60 ps of equilibration and 40 ps of sampling dynamics. The free energy profiles were obtained by combining the statistics from all of the simulations

performed for each reaction using the weighted histogram analysis method (WHAM) [41]. This SCC-DFTB/CHARMM umbrella sampling method has also been applied to creatine–water systems [42].

3. Results and discussion

The purpose of this computational study is to clarify the reaction mechanism of creatinine hydrolysis catalyzed by dizinc enzyme creatininase and to identify the fundamental roles of the two important second-shell residues, His178 and Glu122, together with their neighboring water molecules (Wat1 and Wat2) at the bimetallic center. On the basis of a high-resolution X-ray structure of the EP complex, we first investigate the Michaelis complex by means of QM/MM MD simulations. Then, we present free energy landscapes for path I and II in Scheme 2. The most favorable pathway is further validated by comparing the QM/MM MD simulations of the product resulting from the two different paths with the X-ray structure. The role of Wat2 in catalysis is revealed and the molecular origin of the decreased activity of the E122Q mutant is explained.

3.1 Michaelis Complex and Its Dynamics at Different Protonation States of Glu122.

In order to clarify the most likely protonation state of Glu122, we have conducted two QM/MM MD simulations of the ES complex, with Glu122 either ionized or neutral. Overall, both Michaelis complexes are stable in simulation (Figure S1), with averaged heavy-atom RMSDs of 0.49 ± 0.01 Å (neutral Glu122) and 0.48 ± 0.02 Å (ionized Glu122). Throughout the simulations, creatinine is tightly bound within the enzyme's active site and no changes in the interactions with the zinc ions occur.

While the active site geometries from both simulations (Figure S1B and S1C) are almost the same, the orientation of Glu122 side-chain appears to be different, owing to its

different protonation state. In particular, the simulated structure with the neutral Glu122 best reproduces the initial X-ray structure [11] and maintains a stable hydrogen bond (2.75 ± 0.10 Å), via its carboxylic side-chain, with a neighboring water molecule, Wat2 (Figure S1B). In contrast, we find in the ionized Glu122 system that the loss of this hydrogen bond disfavors the Glu122-Wat2 interaction, leading to a flip of this residue away from the zinc center (Figure S1C). This is similar to what is found in the X-ray crystal structure of the E122Q mutant of creatininase (PDB entry 3A6J [12]). In case of a neutral Glu122, Wat2 places its oxygen atom at a distance of 3.41 ± 0.18 Å from the leaving amide nitrogen, an interaction necessary for proton transfer in path II (see Scheme 2). From these simulations, we can conclude that the neutral form of Glu122 is preferred, and thus used for modeling all WT reaction pathways.

Inspection of the substrate binding interaction within the active site further revealed that the binuclear zinc center (Figure S1B) possesses trigonal-bipyramidal and tetrahedral coordination on Zn1 and on Zn2, respectively. In line with the previous experiments [8, 10], the two zinc ions are located 3.50 ±0.09 Å apart from each other and are ligated by five protein residues (Glu34, His36, Asp45, His120, Glu183), the creatinine substrate and a nucleophilic water molecule (Wat1). The creatinine initially binds through its carbonyl oxygen atom (O_1) to Zn1 in a proximal position (2.38 ± 0.08 Å) that allows polarization of substrate carbonyl group and an increase of the nucleophilicity at C_1. The substrate is anchored (as guided by two water molecules) by interacting with the aromatic rings of Tyr121 and Trp154 and the peptide bonds of Ser78, Tyr121 and Trp174. These interactions place the substrate in a perfect near-attack position to react with the hydroxide ion (Wat1) with a C_1-O_{w1} distance of 2.44 ± 0.13 Å. Wat1 is slightly closer to Zn2 (2.01 ± 0.06 Å) than to Zn1 (Zn1-O_{w1} = 2.11 ± 0.08 Å). Moreover, due to a strong hydrogen bond (2.01 ± 0.07 Å) with a nitrogen atom (N_ε) of the imidazole ring of His178, the orientation of

Wat1 is suitable for direct proton transfer following the proposed ring-opening pathway by Beuth *et al*. (see path I in Scheme 2). Conversely, Wat2 is weakly bound to Zn1 with a relatively long distance (2.87 ± 0.22 Å), but forms three hydrogen bonds with Glu34, Ser78 and Glu122 with O···O distances of ~2.7 Å. These interactions place one of the Wat2 hydrogen atoms (H_{w2}) in a good position for a proton transfer in the proposed pathway by Yoshimoto *et al*. (H_{w2}-N_2 = 2.90 ± 0.22 Å; see path II in Scheme 2). Therefore, given the proximity of the two water molecules (Wat1 and Wat2) with respect to residues His178 and Glu122, respectively, we can conclude that the model with a neutral Glu122 serves as a good starting point for modeling the creatininase reaction via the two reaction pathways (path I and II) shown in Scheme 2.

3.2. Path I.

On the basis of modeling the structure of the water-adduct complex, His178 has been proposed [10] to serve as the proton donor in the ring-opening step, making it functionally equivalent to the common catalytic residue (Asp/Glu) found in the amidohydrolase family [2]. The overall reaction of this pathway is shown in path I of Scheme 2. In order to clarify the possibility of this pathway, we first examined the stationary structures and reaction free-energy for path I using QM/MM reaction path calculations and umbrella sampling MD. The results are illustrated in Figures 1 and 2A. As shown, seven stationary points (ES, TS1, TI1, TS2, I2, TS3, and EP) were identified at the SCC-DFTB/CHARMM22 QM/MM level for path I and their structural parameters are listed in Table 1.

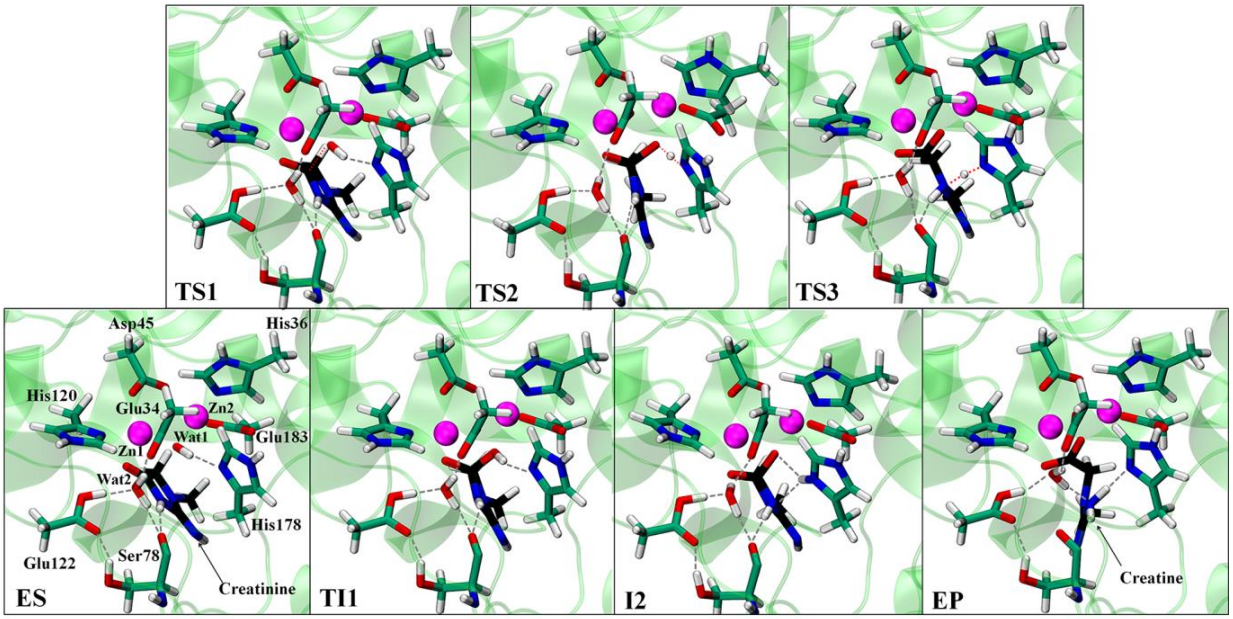

Figure 1. Snapshots of the stationary points obtained from the SCC-DFTB/CHARMM22 reaction path calculations for path I. The substrate is shown in black carbon. Grey dashed lines represent hydrogen bonds, while red dotted lines bond forming and bond breaking.

Path I starts with the nucleophilic addition of the hydroxide ion (Wat1) to the carbonyl carbon atom (C_1) of the substrate amide bond. The attack of the hydroxide readily takes place through transition state 1 (TS1) and forms a *gem-diolate* tetrahedral intermediate 1 (TI1), as evidenced by a drastic decrease of the C_1–O_{w1} distance (2.42 Å at ES → 1.51 Å at TI1). At TS1, the critical C_1–O_{w1} distance is 1.81 Å, and the central C_1 atom is distorted away from its planar geometry observed in ES. Intermediate TI1 features an sp^3 hybridization at C_1, as characterized by the C_1–O_{w1} bond (1.51 Å) and the O_{w1}–C_1–O_1 angle (108.4º). At this stage, the two active site water molecules, hydroxide Wat1 and Wat2, are loosely interacting with zinc cation Zn1 ($Zn1–O_{w1}$ = 2.94 Å; $Zn1–O_{w2}$ = 2.99 Å), while the hydroxide that is now bound to the substrate is still tightly interacting with Zn2 ($Zn2–O_{w1}$ = 2.07 Å). In this step, Wat2 does not participate in any bond forming or bond breaking events and its position

relative to Zn1 remains unperturbed and stabilized by a network of hydrogen bonds, between the conserved residues (Glu34, Ser78 and Glu122) and the *gem-diolate* species.

The *gem-diolate* group of the resulting negatively charged tetrahedral intermediate is well stabilized by the Zn1 ion (see Zn1–O_1, 2.27 Å at ES → 2.01 Å at TI1), and by the imidazole ring nitrogen of His178, (see H_{w1}–N_δ(His178), 2.03 Å at ES → 1.96 Å at TI1). During the TI1 formation, the Zn1 changes its coordination number (CN) from 5 at ES to 4 at TI1, whereas the coordination sphere of Zn2 remains tetrahedral, without significant changes in the position of the ligands. The displacement of the hydroxide ion at the zinc center also results in elongation of the Zn1–Zn2 distance (3.42 Å at ES to 3.69 Å at TI1). It should be noted that the initial penta-coordination of Zn1 enables the Zn^{2+} ion to play multiple catalytic roles, first serving as a Lewis acid to polarize the carbonyl group and later stabilizing the oxyanion formed at the transition state.

In the ring-opening step, the collapse of TI1 involves two sequential proton-transfer processes in which His178 plays a central role as a catalytic base/acid. First, His178 acts as a base and abstracts a proton (H_{w1}) from the hydroxyl group of TI1, generating the doubly deprotonated intermediate 2 (I2) and a protonated His178 (see TI1→I2 in Figure 1). In the next step (I2→EP), the protonated His178 acts as an acid by releasing its received proton to the nitrogen (N_2) atom of the leaving group with the simultaneous breakdown of the C–N bond. At transition state 3 (TS3), the C_1–N_2 bond was elongated at 1.99 Å and the proton (H_{w1}) transferred between the two nitrogen atoms of His178 and of the substrate amide bond was in the middle way (H_{w1}–N_ε(His178) = 1.25 Å and H_{w1}–N_2 = 1.34 Å), indicating a synchronously concerted ring-opening process. This step leads to the cleavage of the scissile amide bond and the generation of the carboxyl (−COOH) and amine ($-NH_2$) terminals of the creatine at EP. The C_1–N_2 distance of 2.34 Å at EP indicates that the creatinine ring is broken. From TI1→ EP, the CN of Zn1 changes from 4 at TI1 to 5 and finally becomes 6 at

EP. In order to restore the active center for another reaction cycle, the product must leave the active center and a second hydroxide ion and substrate must bind in the corresponding positions.

During the whole reaction process, a clear catalytic role of His178 is manifested: it acts first as a general base to abstract a proton from the *gem-diolate* intermediate, and then as a general acid to deliver the proton to the leaving group. Glu122, however, does not directly participate in the reaction, but facilitates the reaction by hydrogen bonding with the second water molecule Wat2 during the initial stage of the reaction. The proton-shuttle process assisted by His178 is similar to the suggested role of an analogous residue, Asp250, in dihydroorotase. [16]

The free-energy profile for path I is shown in Figure 2A. The barrier for the first water-adding step was calculated to be 6.9 kcal/mol and TI1 is found at 3.2 kcal/mol from the ES. The intermediate I2 was calculated to be 5.4 kcal/mol, higher in energy than that of TI1. We find a second transition state (TS2) along the TI1→I2 step with QM/MM free-energy calculations (at SCC-DFTB/CHARMM22 level of theory). TS3 has the highest overall free energy of 18.5 kcal/mol relative to ES, which is in reasonable agreement with the free energy estimated from the experimental rate (~14.1 kcal/mol) [12], considering the limited accuracy of the semiempirical SCC-DFTB method (which can overestimate energy barriers in enzymatic reactions [34]). The overall reaction was exothermic by ~6 kcal/mol.

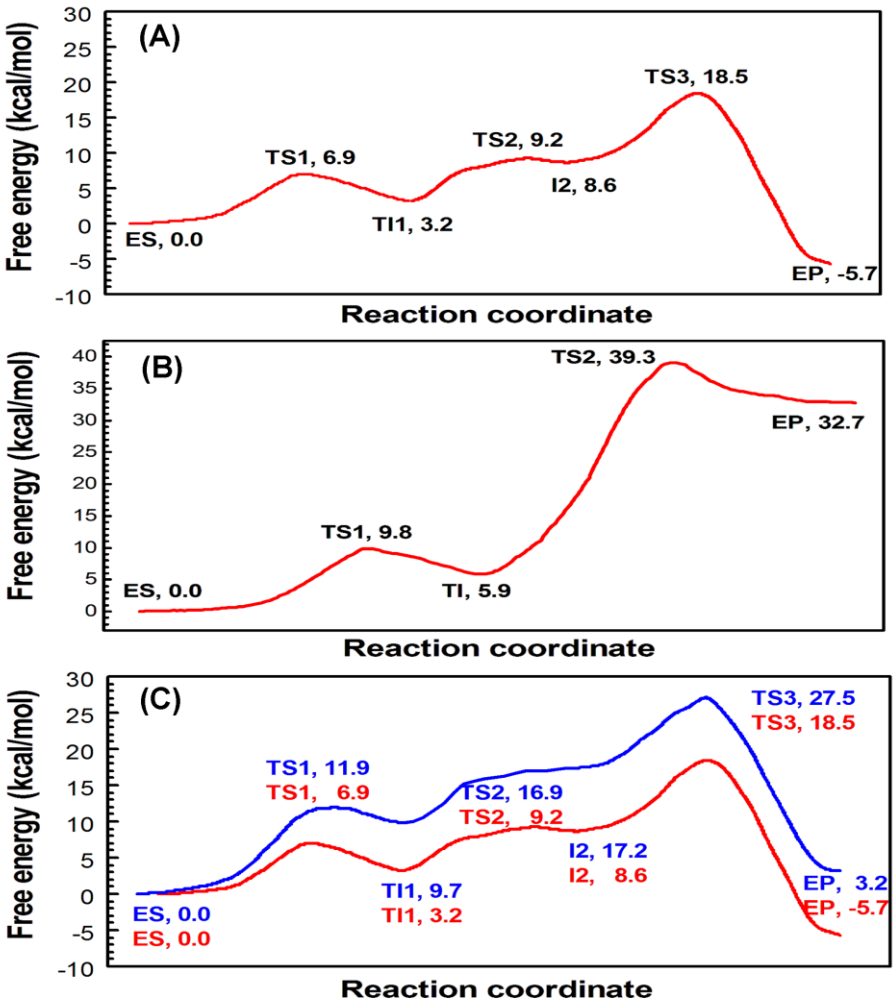

Figure 2. Free energy profiles obtained from SCC-DFTB/CHARMM22 umbrella sampling MD for (A) path I and (B) path II. (C) Comparison of the profiles for path I of WT (red) and E122Q (blue) creatininase.

3.3. Path II.

In path II, the water molecule, Wat2, acts as a base (instead of His178 in path I) by donating one of its protons to the nitrogen leaving group. In this pathway, five stationary points (ES, TS1, TI, TS2, and EP) were identified with the SCC-DFTB/CHARMM22 reaction path calculations (structures are illustrated in Figure 3, relevant geometric parameters are listed in Table 2). In general, the resulting structures of path II are geometrically close to those of path I, but Wat2 is now coordinated to Zn1 with the metal-

ligand interaction shorter than that observed in path I ($Zn1–O_{w2}$; 2.06−2.43 Å for path II and 2.37−2.89 Å for path I).

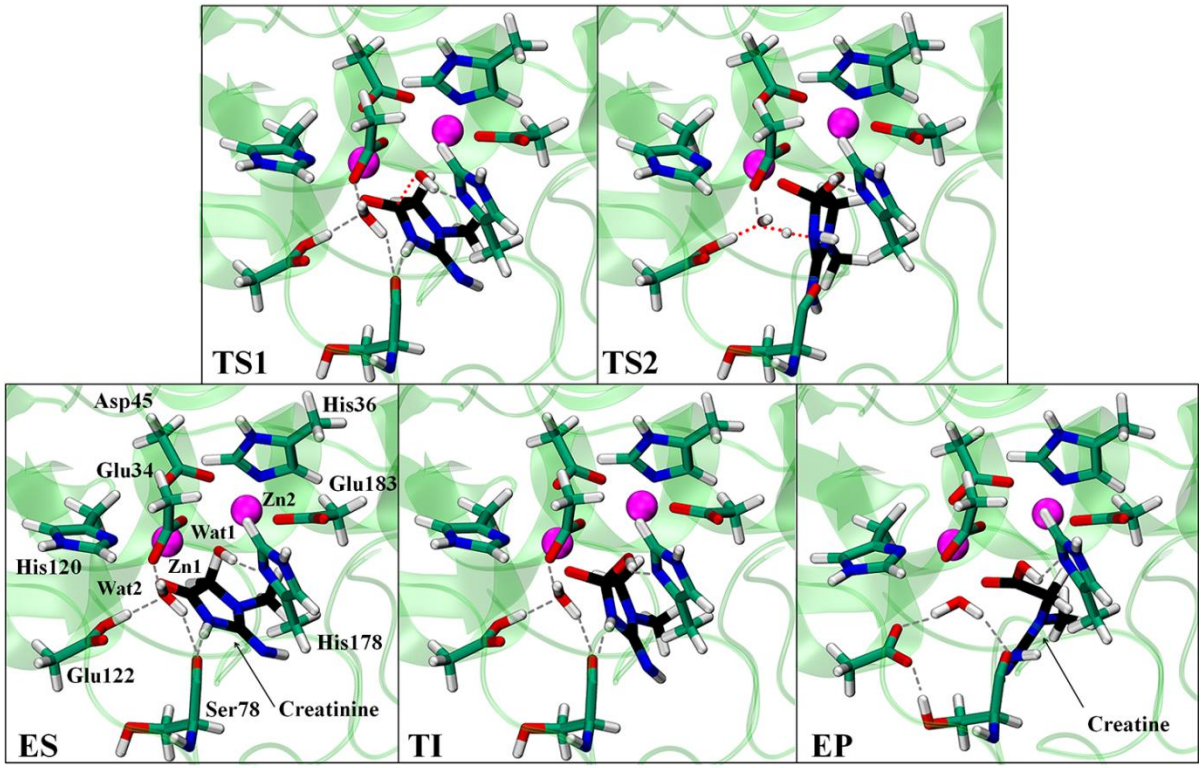

Figure 3. Snapshots of the stationary points obtained from the SCC-DFTB/CHARMM22 reaction path calculations for path II. The substrate is shown with black carbons. Grey dashed lines represent hydrogen bonds, red dotted lines represent bond forming and bond breaking.

From ES → TI, the $C_1–O_w$ is 2.50 Å at ES and is shortening to 1.80 Å at TS1 and then 1.50 Å at TI. This step leads to the generation of the *gem-diolate* intermediate (TI) as indicated by sp^3 characteristics at C_1. In TI, one of the Wat2 protons (H_{w2}) is placed at 2.76 Å from the cyclic amide nitrogen (N_2), setting the stage for proton transfer in the second (ring-opening) step. The Zn1–Zn2 distance is 3.75 Å, which is lengthened by 0.25 Å from the ES (3.48 Å).

In the ring-opening step (TI → EP), the TI collapses by the transfer of the H_{w2} proton (belonging to Wat2) to the nitrogen leaving group. This proton transfer is concerted with the

proton transfer between Glu122 and the deprotonated Wat2, as evidenced by the bond distances, O_{w2}–$H_{\varepsilon 1}$(Glu122), O_{w2}–H_{w2} and H_{w2}–N_2 of 1.29, 1.26, 1.27 Å at TS2, respectively. The reaction is completed by opening of the creatinine ring via C–N bond cleavage, yielding the creatine product with the amine and carboxylic groups at the N– and C–terminal, respectively. This concerted process leads to the cleavage of the cyclic amide bond and regeneration of the second water molecule Wat2. At the EP, the cleaved C–N bond is 2.07 Å, which is significantly different from the distance found in the crystal structure (2.67 Å) [11]. The resulting planar geometry of the carboxylic group of the product is well stabilized through polarization with Zn1 and hydrogen bonding to His178. The position of the newly formed Wat2 molecule is stabilized by hydrogen bonding with two carboxylate groups of Glu122 and Glu34 and the hydroxyl group of creatine product.

The free energy profile for path II (involving water-promoted ring-opening) is shown in Figure 2B. The energy barrier for the first step was calculated to be 9.8 kcal/mol, which is 3 kcal/mol higher than that for the corresponding step of path I (Figure 2A). TS2 presents a barrier height of 39.3 kcal/mol, much higher than the experimentally derived barrier (14.1 kcal/mol). Finally, the product state associated with the ring-opening step shows a relative energy of 32.7 kcal/mol with respect to the ES, indicating that this product state is very unstable. To confirm that this difference reflects a difference in the energies of the ES and EP structures (rather than an artifact of umbrella sampling), we characterized the ES and EP stationary points of both path I and II by DFT calculations on small cluster models (more details in Supporting Information). Estimated $\Delta\Delta G$ value (at the B3LYP/6-31G(d) level) confirms the large difference between the two EP products observed in the free energy profiles obtained from the umbrella sampling simulations.

Note that the difference in energy barrier of the first step for both pathways reflects the variation between different simulations of the same reaction. In any case, TS2 (and EP)

for path II are still very high, indicating this pathway is not realistic; even if one would start from TI1 in path I (3.2 kcal/mol), TS2 for path II is still 36.6 kcal/mol.

3.4 Protonation state of creatine in the enzyme-product complex.

As seen in Figures 1 and 3 and Scheme 2, the products of path I and II yield a creatine molecule with either a carboxylate ($-COO^-$) or carboxylic ($-COOH$) C-terminal, respectively. After the reaction, the product remain in contact with the zinc center via its C-terminal in both cases, but their binding interactions differ significantly: in path II, the protonated oxygen (O_{w1}) of the $-COOH$ group product is detached from Zn1 ($Zn1–O_1$ = 2.25 Å, $Zn1–O_{w1}$ = 3.08 Å) while in path I, the $-COO^-$ group forms a stronger interaction to Zn1 in a bidentate fashion ($Zn1–O_1$ = 2.35 Å, $Zn1–O_{w1}$ = 2.20 Å). In both cases, Zn2 remains tetrahedral with the O_{w1} atom of Wat1 serving as the fourth ligand. In both pathways, the creatine molecule still has relatively short C–N distances (2.34 Å in path I and 2.07 Å in path II), compared to the same distance observed in the crystal structure (2.67 Å) [12]. Based on these observations, it is not clear which form, carboxylate or carboxylic acid C-terminal, is most likely.

To address this issue, two additional 1-ns QM/MM MD simulations were performed for the EP complexes resulting from the two pathways (path I and II, Scheme 2). The selected active-site structures, with the superimposed X-ray structure, are presented in Figure 4 with their structural parameters included in Tables 1-2. The results show that, while the two systems reach equilibrium after 400 ps (Figure S4A), the product from path I is more stable than the one from path II (*i.e.*, a lower heavy-atom RMSD compared to the starting point, Figure S4B). Besides, the scissile C–N bond distance from path I (2.57 ± 0.18 Å) is much closer to that observed in the product X-ray structure (2.67 Å) compared to that from path II (3.13 ± 0.21 Å). Furthermore, the EP active-site conformation during the 1 ns simulation

from path I aligns well with that of the X-ray EP structure, in contrast to that from path II (see Figure 4). Based on these EP simulations, we can conclude that the carboxylate form of the creatine product from path I is more favorable and thus likely represents the true product state.

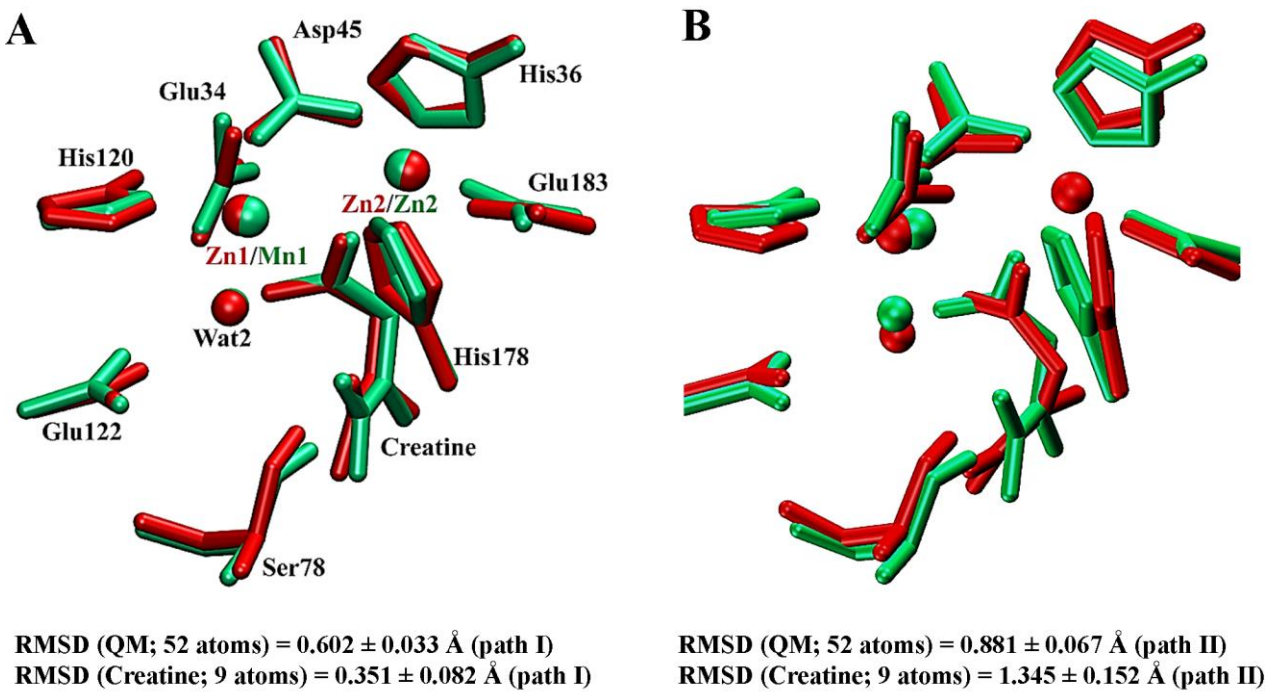

Figure 4. Superposition of the active site of the Mn–Zn creatine product X-ray structure (PDB entry 1V7Z, green) [12] and the Zn–Zn enzyme model (red) complex with (A) carboxylate and (B) carboxylic C–terminal creatine selected from the 1 ns QM/MM MD simulations. RMSD was measured for the QM region (including substrate) during the whole simulation with respect to the X-ray structure.

3.5 Origin of the activity of E122Q mutant and the role of Wat2 in catalysis

It has been shown that Glu122 plays an important role in substrate binding and metal binding in creatinase, and that the mutant E122Q significantly reduces the catalytic activity compared to the wildtype [12]. The authors of this work suggest that the lower activity is due to the loss of a second water molecule bound to Zn1 and hydrogen bonding with the conserved

Glu122, and that water may play a significant role in the final proton-transfer step that leads to the C–N bond cleavage of the substrate.

To understand the effect of the E122Q mutation on catalysis of the reaction, we carried out QM/MM free-energy simulations for path I in the E122Q mutant using the same QM/MM protocol as in the WT calculations (Figure 2C, Figure S5). The E122Q mutant has an increased activation barrier (27.5 kcal/mol *vs* 18.5 kcal/mol) and reaction energy (3.2 kcal/mol *vs* −5.7 kcal/mol) compared to the WT enzyme. The overall mechanism of the mutant remains the same via three reaction steps as in the case of the WT but, in the mutant, I2 is not a minimum and thus no TS2 is located for E122Q. The higher energy of the intermediate I2 in the mutant can be explained by partial disruption of a key H-bond network formed by three conserved residues (Glu34, Ser78, Glu122) and a substrate (see Figures 5A and 5B). Analysis of the radial distribution function (RDF) for (O-O) and (N-O) atomic pairs between the oxygen atom of Wat2 and its nearby residues/substrate further indicates that the Glu → Gln substitution reduces the strength of the H-bond network (Figures 5C and 5D; details of the I2 simulations for the WT and E122Q mutant systems are provided in Figure S6).

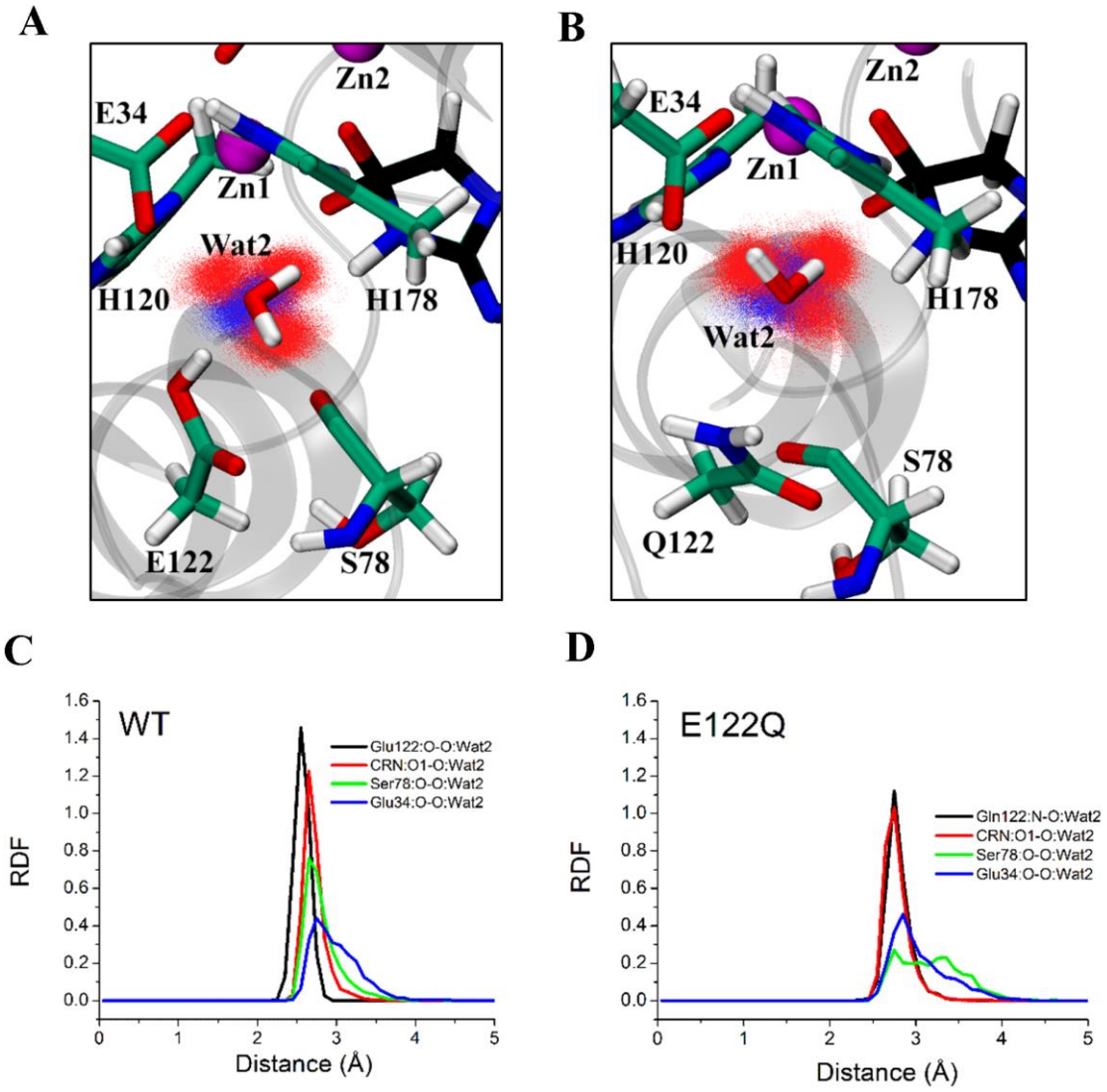

Figure 5. Distribution of a second water molecule (Wat2) in the active site of (A) WT and (B) E122Q creatininase during the 1ns-QM/MM MD simulations of I2. Representative configuration of the active site and Wat2 is depicted, together with the distribution of the Wat2 oxygen (blue dots) and hydrogens (red dots). (C−D) Radial distribution function (RDF) of Wat2 around the three conserved hydrogen bonding residues (Glu/Gln122, Ser78, Glu34) and the O_1 atom of the creatinine substrate (labelled as CRN) for WT and E122Q.

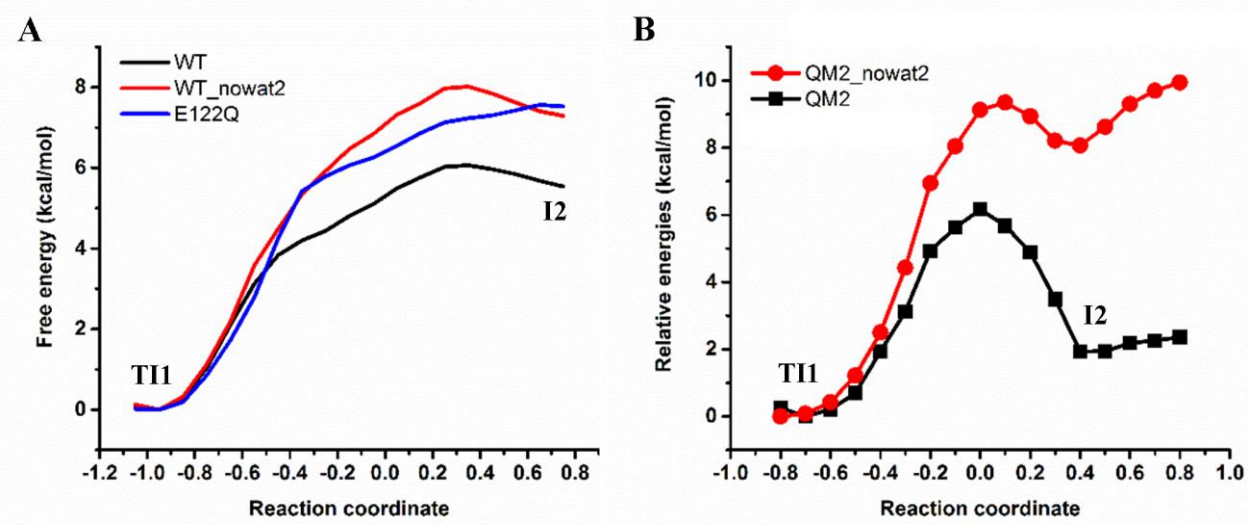

Figure 6. (A) QM/MM (SCC-DFTB/CHARMM22) free-energy and (B) QM gas-phase energy profiles with and without Wat2 (denoted as WT, WT_nowat2, QM2 and QM2_nowat2, respectively) for the second step (TI1→I2) of path I. Gas-phase energy profiles were obtained from B3LYP/6-31G(d)//SCC-DFTB single-point energy calculations using a model larger than the QM region extracted from QM/MM potential energy profile (see Figure S7).

To better understand the role of Glu122 in stabilizing I2 via this water molecule (Wat2), we repeated the simulation of the TI1→I2 step of the WT pathway I using both QM/MM and DFT QM models, but without Wat2 present (Figure 6). Comparison of the energy barriers obtained at TS2 with and without Wat2 (6 kcal/mol and 8 kcal/mol for QM/MM and 6 kcal/mol and 9 kcal/mol for QM, respectively) shows that the barrier increases by at least 2 kcal/mol in the absence of the water. This indicates that catalysis of the reaction from TI1 to I2 is dependent on Wat2 and that Wat2 and Glu122 play a critical role in intermediate stabilization. Wat2 in its proper orientation, which is directly controlled by the three conserved residues (Glu34, Ser78, Glu122), provides an effective stabilization of the negative charge of O_1 in I2 (see Figure 5), resulting in a lower energy barrier (and reaction

energy) of the computed profile in Figure 2C. Based on our finding, we suggest a revised mechanism based on path I for the reaction catalyzed by creatininase (Scheme 3), which involves the attack of zinc-bound water onto the substrate carbonyl carbon, followed by a proton transfer from the μ-hydroxide to the N_ε atom of His178 and finally the breakdown of the creatinine ring as a result of the proton transfer from the protonated His178 to the substrate amide bond.

Scheme 3: Suggested creatinine hydrolysis mechanism based on the present calculations

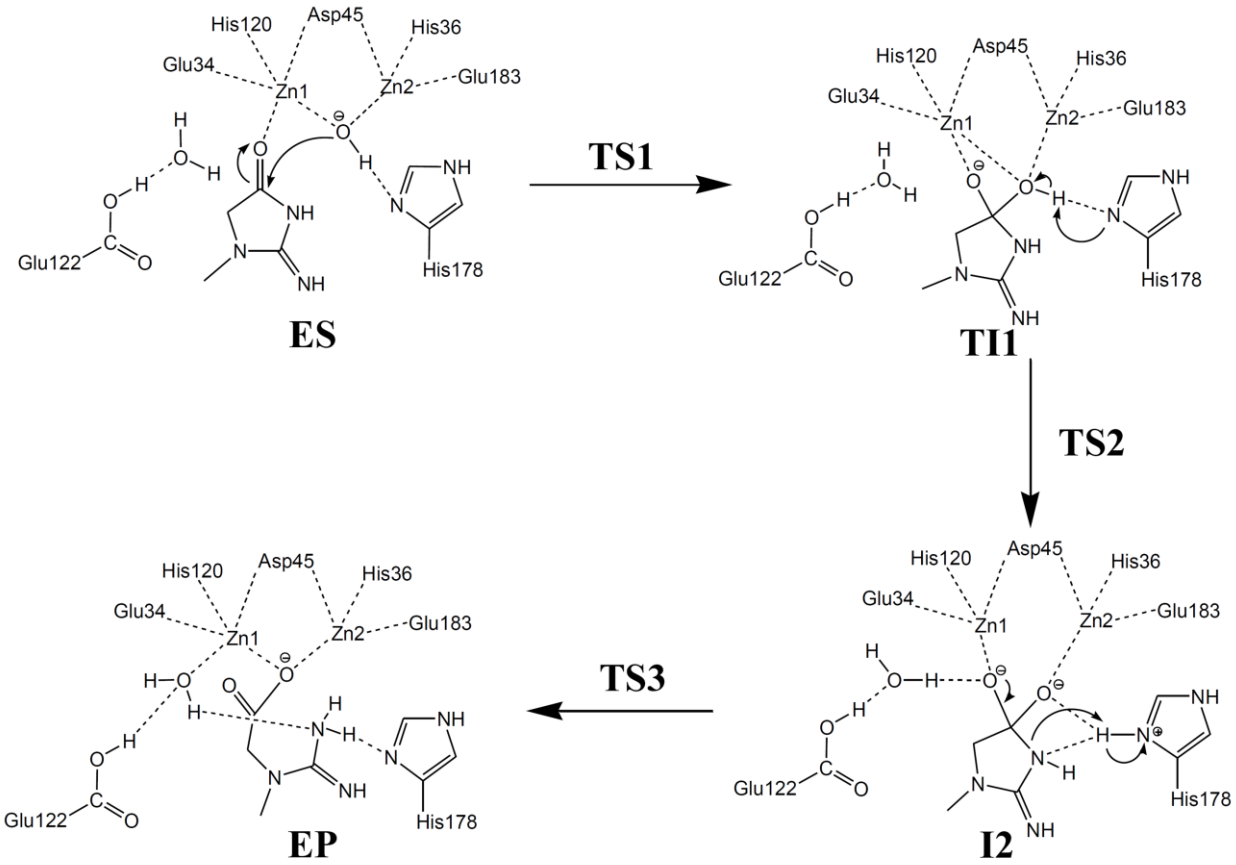

The reaction pathway proposed herein (path I) resembles the mechanism characterized previously [16] for the hydrolysis of dihydroorotate catalyzed by dihydroorotase, a dinuclear zinc enzyme that also belongs to the amidohydrolase superfamily. In this reaction pathway, the bridged water molecule acts as a nucleophile,

and Asp250 performs a catalytic role very similar to the role we assign here to His178 herein. Interestingly, the rate-limiting step (energy barrier of 19.7 kcal/mol) corresponds to the protonation of the amide nitrogen by Asp250 coupled with the amide bond cleavage. This step is analogous to the third step of path I presented here, with a very similar free energy barrier (18.5 kcal/mol). These similarities confirm that both enzymes, which act on different substrates, share a highly similar catalytic mechanism, and that path I is indeed the most likely pathway for the reaction catalyzed by creatininase.

4. Conclusions

The reversible conversion of creatinine to creatine via a ring-opening mechanism catalyzed by the binuclear zinc enzyme creatininase was investigated by using SCC-DFTB/CHARMM22 QM/MM and DFT(B3LYP) methods. Two reaction pathways in which either His178 or Wat2 serves as a proton donor in the ring-opening step were considered. Our calculations give strong support to the His178-promoted ring-opening pathway where the conserved His178 serves as a general base/acid to shuttle a proton from tetrahedral intermediate to nitrogen leaving group, leading to the creatine product, via a stepwise mechanism. The overall activation barrier is in good agreement with the experimental rate.

We find that the crystallographic water molecule Wat2 (bound to Glu34, Glu122, Ser78 and Zn1) has a notable catalytic effect beside its role in substrate binding: it stabilizes the reaction by 2-3 kcal/mol. The simulations demonstrate that Glu122 contributes by assisting the catalytic role of Wat2, explaining why the E122Q mutation decreases (but not abolishes) the enzyme reaction rate: Glu122 keeps Wat2 in a suitable position to interact with the reacting species. Further, the QM/MM simulations show that this interaction is only possible when Glu122 is protonated.

In summary, the study clarifies the catalytic role played by His178 and Glu122 during the enzymatic reaction catalyzed by creatininase: His178 acts as a dual Lewis acid/base, whereas Glu122 is not directly involved in the chemical process but plays a role in stabilizing the transition state and orienting the position of its neighboring water molecule, which acts to stabilize the oxyanion. Our simulations reported here therefore support the earlier proposal [10] for the role of His178 as a proton donor and the revised mechanism proposed is consistent with the available crystallographic and mutagenesis studies [12].

ACKNOWLEDGEMENTS

This work was supported by grants from the University of Phayao (Grant Nos. R020056216016 and RD59008) and the Thailand Research Fund (Grant Nos. MRG5680143 and TRG5880241). J.J. thanks the National e-Science Infrastructure Consortium (URL: http://www.e-science.in.th) for computer time. J.I.M. acknowledges the Spanish Ministerio de Ciencia e Innovación (CTQ2015-67608-P) for funding. M.W.vdK. is a BBSRC David Phillips Fellow and thanks BBSRC for support (Grant No. BB/M026280/1). A.J.M. acknowledges funding from the EPSRC (EP/M022609/1).

Supporting Information

RMSD plots during the ES simulations of the Glu122 ionized and neutral systems; illustration of the reaction coordinate (RC) chosen for each step of the reaction under study; analysis of zinc bound and unbound states of Wat2 during the EP simulations of path I; RMSD plots during the EP simulations of path I and II; snapshots of the reaction of the E122Q mutant; results of the I2 simulations for the E122Q system and the WT system with and without Wat2; comparison of different QM treatments between SCC-DFTB with B3LYP/6-31G(d) for the step TI1→I2 of path I; the $\Delta\Delta G$ value estimated from small cluster

DFT calculations. This material is available free of charge via the Internet at http://pubs.acs.org.

References

1. Holm, L., and Sander, C. (1997) An evolutionary treasure: unification of a broad set of amidohydrolases related to urease, *Proteins: Struct., Funct., Bioinf. 28*, 72-82.
2. Seibert, C. M., and Raushel, F. M. (2005) Structural and catalytic diversity within the amidohydrolase superfamily, *Biochemistry 44*, 6383-6391.
3. Thoden, J. B., Phillips, G. N., Neal, T. M., Raushel, F. M., and Holden, H. M. (2001) Molecular structure of dihydroorotase: A paradigm for catalysis through the use of a binuclear metal center, *Biochemistry 40*, 6989-6997.
4. Kim, G. J., and Kim, H. S. (1998) Identification of the structural similarity in the functionally related amidohydrolases acting on the cyclic amide ring, *Biochem. J. 330*, 295-302.
5. Szulmajster, J. (1958) Bacterial degradation of creatinine. II. Creatinine desimidase, *Biochimica et biophysica acta 30*, 154-163.
6. Wyss, M., and Kaddurah-Daouk, R. (2000) Creatine and creatinine metabolism, *Physiol. Rev. 80*, 1107-1213.
7. Tsuru, D., Oka, I., and Yoshimoto, T. (1976) Creatinine decomposing enzymes in Pseudomonas putida, *Agric. Biol. Chem. 40*, 1011-1018.
8. Rikitake, K., Oka, I., Ando, M., Yoshimoto, T., and Tsuru, D. (1979) Creatinine amidohydrolase (creatininase) from Pseudomonas putida. Purification and some properties, *J. Biochem. 86*, 1109-1117.
9. Beuth, B., Niefind, K., and Schomburg, D. (2002) Crystallization and preliminary crystallographic analysis of creatininase from Pseudomonas putida, *Acta Crystallogr. Sect. D-Biol. Crystallogr. 58*, 1356-1358.
10. Beuth, B., Niefind, K., and Schomburg, D. (2003) Crystal structure of creatininase from Pseudomonas putida: a novel fold and a case of convergent evolution, *J. Mol. Biol. 332*, 287-301.
11. Yoshimoto, T., Tanaka, N., Kanada, N., Inoue, T., Nakajima, Y., Haratake, M., Nakamura, K. T., Xu, Y., and Ito, K. (2004) Crystal structures of creatininase reveal the substrate binding site and provide an insight into the catalytic mechanism, *J. Mol. Biol. 337*, 399-416.
12. Yamashita, K., Nakajima, Y., Matsushita, H., Nishiya, Y., Yamazawa, R., Wu, Y. F., Matsubara, F., Oyama, H., Ito, K., and Yoshimoto, T. (2010) Substitution of Glu122 by glutamine revealed the function of the second water molecule as a proton donor in the binuclear metal enzyme creatininase, *J. Mol. Biol. 396*, 1081-1096.
13. Kim, H., and Lipscomb, W. N. (1993) Differentiation and identification of the two catalytic metal binding sites in bovine lens leucine aminopeptidase by X-ray crystallography, *Proc. Natl. Acad. Sci. U. S. A. 90*, 5006-5010.
14. Valdez, C. E., and Alexandrova, A. N. (2012) Why urease is a di-nickel enzyme whereas the CcrA β-lactamase is a di-zinc enzyme, *J. Phys. Chem. B 116*, 10649-10656.
15. Wong, K. Y., and Gao, J. (2007) The reaction mechanism of paraoxon hydrolysis by phosphotriesterase from combined QM/MM simulations, *Biochemistry 46*, 13352-13369.

16. Rong-Zhen Liao, Jian-Guo Yu, Frank M. Raushel, and Himo, F. (2008) Theoretical investigation of the reaction mechanism of the dinuclear zinc enzyme dihydroorotase, *Chem. Eur. J. 14*, 4287 – 4292.
17. Chen, Y., Farquhar, E. R., Chance, M. R., Palczewski, K., and Kiser, P. D. (2012) Insights into substrate specificity and metal activation of mammalian tetrahedral aspartyl aminopeptidase, *J. Biol. Chem. 287*, 13356-13370.
18. Abendroth, J., Niefind, K., and Schomburg, D. (2002) X-ray structure of a dihydropyrimidinase from Thermus sp. at 1.3 Å resolution, *J. Mol. Biol. 320*, 143-156.
19. Gilboa, R., Spungin-Bialik, A., Wohlfahrt, G., Schomburg, D., Blumberg, S., and Shoham, G. (2001) Interactions of Streptomyces griseus aminopeptidase with amino acid reaction products and their implications toward a catalytic mechanism, *Proteins: Struct. Funct. Bioinf. 44*, 490-504.
20. Lee, V. S., Kodchakorn, K., Jitonnom, J., Nimmanpipug, P., Kongtawelert, P., and Premanode, B. (2010) Influence of metal cofactors and water on the catalytic mechanism of creatininase-creatinine in aqueous solution from molecular dynamics simulation and quantum study, *J. Comput. Aided. Mol. Des. 24*, 879-886.
21. Olsson, M. H., Sondergaard, C. R., Rostkowski, M., and Jensen, J. H. (2011) PROPKA3: consistent treatment of internal and surface residues in empirical pKa predictions, *J. Chem. Theory Comput. 7*, 525-537.
22. Hooft, R. W., Sander, C., and Vriend, G. (1996) Positioning hydrogen atoms by optimizing hydrogen-bond networks in protein structures, *Proteins 26*, 363-376.
23. Elstner, M., Porezag, D., Jungnickel, G., Elsner, J., Haugk, M., Frauenheim, T., Suhai, S., and Seifert, G. (1998) Self-consistent-charge density-functional tight-binding method for simulations of complex materials properties, *Phys. Rev. B 58*, 7260-7268.
24. MacKerell, A. D., Bashford, D., Bellott, M., Dunbrack, R. L., Evanseck, J. D., Field, M. J., Fischer, S., Gao, J., Guo, H., Ha, S., Joseph-McCarthy, D., Kuchnir, L., Kuczera, K., Lau, F. T. K., Mattos, C., Michnick, S., Ngo, T., Nguyen, D. T., Prodhom, B., Reiher, W. E., Roux, B., Schlenkrich, M., Smith, J. C., Stote, R., Straub, J., Watanabe, M., Wiórkiewicz-Kuczera, J., Yin, D., and Karplus, M. (1998) All-atom empirical potential for molecular modeling and dynamics studies of proteins, *J. Phys. Chem. B 102*, 3586-3616.
25. Jorgensen, W. L., Chandrasekhar, J., Madura, J. D., Impey, R. W., and Klein, M. L. (1983) Comparison of simple potential functions for simulating liquid water, *J. Chem. Phys. 79*, 926.
26. Elstner, M., Cui, Q., Munih, P., Kaxiras, E., Frauenheim, T., and Karplus, M. (2003) Modeling zinc in biomolecules with the self consistent charge-density functional tight binding (SCC-DFTB) method: applications to structural and energetic analysis, *J. Comput. Chem. 24*, 565-581.
27. Cui, Q., Elstner, M., Kaxiras, E., Frauenheim, T., and Karplus, M. (2001) A QM/MM implementation of the self-consistent charge density functional tight binding (SCC-DFTB) method, *J. Phys. Chem. B 105*, 569-585.
28. Xu, Q., Guo, H. B., Wlodawer, A., Nakayama, T., and Guo, H. (2007) The QM/MM molecular dynamics and free energy simulations of the acylation reaction catalyzed by the serine-carboxyl peptidase kumamolisin-As, *Biochemistry 46*, 3784-3792.
29. Xu, D., and Guo, H. (2009) Quantum mechanical/molecular mechanical and density functional theory studies of a prototypical zinc peptidase (carboxypeptidase A) suggest a general acid-general base mechanism, *J. Am. Chem. Soc. 131*, 9780-9788.

30. Wu, S., Xu, D., and Guo, H. (2010) QM/MM studies of monozinc beta-lactamase CphA suggest that the crystal structure of an enzyme-intermediate complex represents a minor pathway, *J. Am. Chem. Soc. 132*, 17986-17988.
31. Wu, S., Zhang, C., Xu, D., and Guo, H. (2010) Catalysis of carboxypeptidase A: promoted-water versus nucleophilic pathways, *J. Phys. Chem. B 114*, 9259-9267.
32. Xu, Q., Li, L., and Guo, H. (2010) Understanding the mechanism of deacylation reaction catalyzed by the serine carboxyl peptidase kumamolisin-As: insights from QM/MM free energy simulations, *J. Phys. Chem. B 114*, 10594-10600.
33. Jitonnom, J., Lee, V. S., Nimmanpipug, P., Rowlands, H. A., and Mulholland, A. J. (2011) Quantum mechanics/molecular mechanics modeling of substrate-assisted catalysis in family 18 chitinases: conformational changes and the role of Asp142 in catalysis in ChiB, *Biochemistry 50*, 4697-4711.
34. Jitonnom, J., Limb, M. A., and Mulholland, A. J. (2014) QM/MM free-energy simulations of reaction in Serratia marcescens chitinase B reveal the protonation state of Asp142 and the critical role of Tyr214, *J. Phys. Chem. B 118*, 4771-4783.
35. Brooks, C. L., and Karplus, M. (1983) Deformable stochastic boundaries in molecular dynamics, *J. Chem. Phys. 79*, 6312.
36. Ryckaert, J.-P., Ciccotti, G., and Berendsen, H. J. C. (1977) Numerical integration of the cartesian equations of motion of a system with constraints: molecular dynamics of n-alkanes, *J. Comp. Phys. 23*, 327-341.
37. Brooks, B. R., Bruccoleri, R. E., Olafson, B. D., States, D. J., Swaminathan, S., and Karplus, M. (1983) CHARMM: A program for macromolecular energy, minimization, and dynamics calculations, *J. Comput. Chem. 4*, 187-217.
38. Ribeiro, A. J. M., Santos-Martins, D., Russo, N., Ramos, M. J., and Fernandes, P. A. (2015) Enzymatic flexibility and reaction rate: a QM/MM study of HIV-1 protease, *ACS Catal. 5*, 5617-5626.
39. Lodola, A., Sirirak, J., Fey, N., Rivara, S., Mor, M., and Mulholland, A. J. (2010) Structural fluctuations in enzyme-catalyzed reactions: determinants of reactivity in fatty acid amide hydrolase from multivariate statistical analysis of quantum mechanics/molecular mechanics paths., *J. Chem. Theory Comput. 6*, 2948-2960.
40. Woodcock, H. L., Hodošček, M., and Brooks, B. R. (2007) Exploring SCC-DFTB paths for mapping QM/MM reaction mechanisms, *J. Phys. Chem. A 111*, 5720-5728.
41. Kumar, S., Rosenberg, J. M., Bouzida, D., Swendsen, R. H., and Kollman, P. A. (1992) THE weighted histogram analysis method for free-energy calculations on biomolecules. I. The method, *J. Comput. Chem. 13*, 1011-1021.
42. Ivchenko, O., Whittleston, C. S., Carr, J. M., Imhof, P., Goerke, S., Bachert, P., and Wales, D. J. (2014) Proton transfer pathways, energy landscape, and kinetics in creatine-water systems, *J. Phys. Chem. B 118*, 1969-1975.

Table 1. Structural Parameters of Stationary Points Obtained from the QM/MM Reaction Path Calculation for Path I

Distance (Å), Angle (°)	QM/MM Reaction Path							MD (EP) [c]	Exp[a]
	ES	TS1	TI1	TS2	I2	TS3	EP		
C_1–O_{w1}	2.42	1.81	1.51	1.48	1.47	1.37	1.34	1.33 ± 0.03	1.26
O_{w1}–N_{ε}(His178)	2.95	2.92	2.89	2.57	2.72	2.97	3.14	3.13 ± 0.21	3.03
H_{w1}–N_{ε}(His178)	2.03	1.98	1.96	1.14	1.05	1.25	2.04	2.23 ± 0.22	–
H_{w1}–N_2	2.97	2.54	2.46	2.59	2.02	1.34	1.04	1.04 ± 0.03	–
C_1–N_2	1.36	1.39	1.43	1.45	1.46	1.99	2.34	2.57 ± 0.18	2.67
C_1–O_1	1.26	1.34	1.40	1.44	1.42	1.31	1.24	1.26 ± 0.02	1.25
O_{w2}–N_2	3.30	3.31	3.44	3.38	3.33	3.20	2.99	3.12 ± 0.20	3.02
O_{w2}–$O_{\varepsilon 2}$(Glu34)	2.70	2.76	2.80	2.94	2.97	2.72	2.72	2.71 ± 0.11	2.78
O_{w2}–$O_{\varepsilon 1}$(Glu122)	2.64	2.63	2.61	2.43	2.42	2.59	2.71	2.71 ± 0.12	2.66
Zn1–O_{w2}	2.89	3.03	2.99	3.11	3.18	2.88	2.39	2.44 ± 0.20	2.28[b]
Zn1–O_{w1}	2.09	2.36	2.94	2.39	2.22	2.25	2.20	2.22 ± 0.10	2.27[b]
Zn1–O_1	2.27	2.05	2.01	2.15	2.24	2.21	2.35	2.48 ± 0.13	2.38[b]
Zn1–$O_{\varepsilon 1}$(Asp45)	2.13	2.12	2.15	2.08	2.08	2.12	2.11	2.12 ± 0.06	2.06[b]
Zn1–$O_{\varepsilon 1}$(Glu34)	2.15	2.06	2.05	2.08	2.12	2.12	2.07	2.10 ± 0.08	2.08[b]
Zn1–N_{ε}(His120)	2.07	2.03	2.02	2.04	2.03	2.01	2.00	2.01 ± 0.06	2.27[b]
Zn1–Zn2	3.42	3.74	3.69	3.51	3.49	3.66	3.62	3.67 ± 0.13	3.56[b]
Zn2–O_{w1}	1.99	2.01	2.07	2.03	2.01	1.99	2.01	2.04 ± 0.07	1.94
Zn2–$O_{\varepsilon 2}$(Asp45)	2.14	2.11	2.05	2.09	2.11	2.11	2.12	2.09 ± 0.07	1.97
Zn2–N_{δ}(His36)	1.99	1.97	1.97	1.97	1.98	1.96	1.95	1.95 ± 0.05	2.01
Zn2–O_{ε}(Glu183)	2.05	2.04	2.04	2.04	2.03	2.03	2.03	2.02 ± 0.06	2.00
O_{w1}–C_1–O_1	86.3	103.9	108.4	105.9	105.8	112.7	114.8	116.9 ± 2.6	122.1
N2–C3–N4–C5	3.2	–10.4	–0.3	6.1	5.9	5.4	0.6	–3.0 ± 12.2	1.47
C3–N4–C5–C1	–5.2	12.2	–11.7	–9.4	–4.5	–9.0	–13.3	–37.9 ± 18.9	–38.0

[a] Values taken from the crystal structure of EP complex (PDB entry 1V7Z)

[b] Mn1-ligand

[c] Average values obtained from 600−1000 ps of the EP simulation of *Wat2_bound* state (see details in Figure S3)

Table 2. Structural Parameters of Stationary Points Obtained from the QM/MM Reaction Path Calculation for Path II

Distance (Å), Angle (°)	QM/MM Reaction Path					MD (EP)	Exp[a]
	ES	TS1	TI	TS2	EP		
C_1–O_{w1}	2.50	1.80	1.50	1.47	1.43	1.43 ± 0.04	1.26
O_{w1}–N_{ε}(His178)	2.97	2.93	2.91	2.80	2.65	2.84 ± 0.18	3.03
H_{w1}–N_{ε}(His178)	1.99	1.98	1.98	2.00	2.05	2.13 ± 0.33	–
H_{w1}–N_2	3.05	2.44	2.44	2.51	2.76	2.70 ± 0.14	–
C_1–N_2	1.36	1.40	1.43	1.51	2.07	3.13 ± 0.21	2.67
C_1–O_1	1.25	1.32	1.40	1.37	1.25	1.24 ± 0.02	1.25
O_{w2}–H_{w2}	0.98	0.98	0.98	1.26	3.16	3.16 ± 0.01	–
H_{w2}–N_2	2.84	2.73	2.76	1.27	1.03	1.04 ± 0.03	–
O_{w2}–N_2	3.34	3.25	3.28	2.51	3.05	3.16 ± 0.18	3.02
O_{w2}–$H_{\varepsilon 1}$(Glu122)	1.71	1.70	1.68	1.29	1.03	1.03 ± 0.03	–
$H_{\varepsilon 1}$(Glu122)–$O_{\varepsilon 1}$(Glu122)	1.01	1.01	1.01	1.13	1.58	1.58 ± 0.01	–
O_{w2}–$O_{\varepsilon 2}$(Glu34)	2.66	2.64	2.64	2.81	2.71	2.79 ± 0.14	2.78
O_{w2}–$O_{\varepsilon 1}$(Glu122)	2.72	2.71	2.68	2.42	2.60	2.59 ± 0.03	2.66
Zn1–O_{w2}	2.43	2.40	2.20	2.06	2.16	2.20 ± 0.08	2.28[b]
Zn1–O_{w1}	2.05	2.33	2.90	3.12	3.08	3.15 ± 0.16	2.27[b]
Zn1–O_1	2.40	2.21	2.02	2.04	2.25	2.29 ± 0.11	2.38[b]
Zn1–$O_{\varepsilon 1}$(Asp45)	2.22	2.20	2.32	2.36	2.17	2.13 ± 0.07	2.06[b]
Zn1–O_{ε}(Glu34)	2.16	2.13	2.13	2.08	2.11	2.08 ± 0.07	2.08[b]
Zn1–N_{ε}(His120)	2.06	2.04	2.01	2.00	1.96	1.98 ± 0.05	2.27[b]
Zn1–Zn2	3.48	3.65	3.75	3.76	3.70	3.94 ± 0.17	3.56[b]
Zn2–O_{w1}	2.00	2.04	2.05	2.11	2.16	2.18 ± 0.08	1.94
Zn2–$O_{\varepsilon 2}$(Asp45)	2.13	2.10	2.04	2.02	2.08	2.04 ± 0.07	1.97
Zn2–N_{δ}(His36)	1.97	1.96	1.95	1.95	1.93	1.94 ± 0.05	2.01
Zn2–O_{ε}(Glu183)	2.02	2.01	2.03	2.03	2.03	2.01 ± 0.07	2.00

[a] Values taken from the crystal structure of EP complex (PDB entry 1V7Z)

[b] Mn1-ligand

TOC graphic

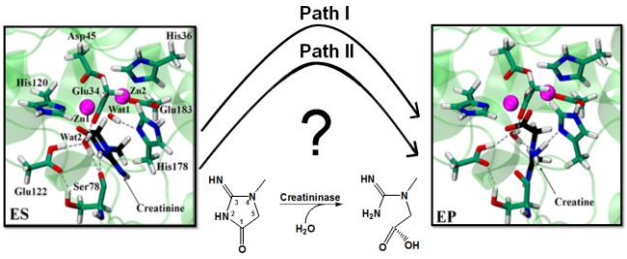
Path I
Path II
?
Asp45
His36
His120
Glu34
Zn2
Zn1
Wat1
Glu183
Wat2
His178
Glu122
Ser78
Creatinine
ES
Creatininase
H_2O
Creatine
EP